Available online at www.sciencedirect.com
SCIENCE DIRECT®
Energy Conversion and Management 46 (2005) 313–334
ENERGY CONVERSION & MANAGEMENT
www.elsevier.com/locate/enconman

Static and dynamic flow instability of a parallel microchannel heat sink at high heat fluxes

Jinliang Xu *, Jijun Zhou, Yunhua Gan

Guangzhou Institute of Energy Conversion, Chinese Academy of Sciences, Wushan, Guangzhou 510640, PR China

Received 6 December 2003; accepted 4 February 2004
Available online 16 March 2004

Abstract

Experiments were conducted to measure the onset of flow instability (OFI) (static flow instability) and dynamic unsteady flow in a compact heat sink consisting of 26 rectangular microchannels with 300 μm width and 800 μm depth. The planform area is 5.0×1.53 cm^2. Tests were performed with water and methanol as working fluids with mass fluxes of 20–1200 kg/m^2 s, inlet temperatures of 30, 50 and 70 °C and effective heating powers of 100–450 W. It was found that the onset of flow instability occurs at the outlet temperature of 93–96 °C, which was several degrees lower than the saturated temperature of 100 °C corresponding to the exit pressure. Fine bubbles were detected close to the channel exit, and they were moving out of the channel to form a unit circular bubble in the outlet plenum. Once the mass flux is lower than that of OFI, three types of oscillations were identified: large amplitude/long period oscillation superimposed with small amplitude/short period oscillation and small amplitude/short period oscillation. Thermal oscillations were always accompanying the above two oscillations. Observations through the microscope and physical explanations were given corresponding to the above oscillation flows. Similar tests were also performed with methanol as working fluid.

Keywords: Microchannel; Onset of flow instability; Large amplitude/long period oscillation; Small amplitude/short period oscillation; Thermal oscillation

1. Introduction

In recent years, due to the high demand of electronic cooling, thermal management packaging system and bio-MEMS applications, flow and heat transfer in microchannels have been receiving

* Corresponding author. Tel./fax: +86-20-87057656/87624728.
E-mail address: xujl@ms.giec.ac.cn (J. Xu).

0196-8904/$ - see front matter © 2004 Elsevier Ltd. All rights reserved.
doi:10.1016/j.enconman.2004.02.012

Nomenclature

A_C	cross-section area of one microchannel
A_t	area of planform surface (top)
$C_{P,f}$	specific heat
D_e	hydraulic diameter of microchannel
G	mass flux
G_{sat}	mass flux at saturated liquid exit condition
h_{in}	liquid enthalpy corresponding to inlet liquid temperature
h_{tp}	heat transfer coefficient
H_{fg}	latent heat of evaporation
H_{w1}	thickness of glass cover plate
H_{w2}	depth from bottom wall to locations where thermocouple wires are located
H_{ch}	depth of microchannel
H_{cell}	depth from top cover plate surface to locations where thermocouple wires are located
k_s	solid wall thermal conductivity
m	fin parameter
N	total number of microchannels
P_{in}	inlet pressure
q_{eff}	effective heat flux
$q_{eff,OFI}$	effective heat flux at OFI condition
q''_{sat}	heat flux leading to exit saturated liquid condition
Q	effective heating power
t_1	time at which microchannels switch from one cycle to another cycle
t_2	time at which microchannels switch from one cycle to another cycle
t_A	time at which fine bubbles are detected close to channel exit
t_B	time at which vapor–liquid interface reaches entrance of the microchannels
t_C	time at which vapor–liquid interface moves downstream and close to channel exit and new cycle begins
T_{in}	inlet fluid temperature
T_f	fluid temperature
T_{sat}	saturated temperature
T_w	wall temperatures where thermocouple wires are located
$T_{w,in}$	bottom wall temperature
V	volume flow rate
W_{ch}	width of microchannel
W_w	half width between neighboring microchannels
η	fin efficiency
ρ_f	liquid density
ρ_g	vapor density
σ	surface tension

great attention. A microchannel heat sink is very attractive for high heat flux situations due to its larger area to volume ratio. Heat transfer is greatly enhanced. Compared with single phase liquid flow in microchannels, a boiling two phase microchannel heat sink has the following advantages [1]:

- A two phase microchannel heat sink relies on the latent heat of evaporation which keeps both the uniform fluid and solid wall temperatures at the coolant saturation temperature level along the flow direction.
- A two phase microchannel heat sink also needs less coolant flow rate, and thus, a compact coolant pump with small capacity can be used.

However, two phase flow and heat transfer in microchannels is quite different from single phase liquid flow. A recent review by Kandlikar [2] shows that a lot of issues must be covered in order to design an effective micro-evaporator. These include pressure drop, heat transfer coefficient, flow pattern, two phase flow instability and critical heat flux. At this stage, most of the existing work on microchannel flow boiling has been focused on the stable flow boiling heat transfer process. However, two phase flow instability is of great concern for the microchannel heat sink, consisting of both the static flow instability and the dynamic one. The static flow instability can be characterized in terms of the demand curve of the pressure drop against the flow rate. The onset of flow instability (OFI) is identified as the minimum of the demand curve. A lower flow rate than that of the OFI leads to flow rate excursions between single phase liquid flow and two phase flow.

1.1. Onset of flow instability (static flow instability)

The appearing of the OFI generally relates to the increased voidage in the channels, leading to increased pressure drop. For larger channels, the OFI always takes place at a flow rate that is slight lower than that of the onset of significant void (OSV).

The onset of nucleate boiling (ONB) and onset of significant void have been studied extensively in the past, resulting in successful empirical correlations and semi-analytical models [3]. However, when the channel size satisfies the criterion of $D_e < \sqrt{\sigma/g(\rho_f - \rho_g)}$, the surface tension plays an important role that leads to a different mechanism in microchannels. Little has been done on the onset of flow instability for the microchannel system. Recently, Kennedy et al. [3] studied the onset of flow instability in a circular tube with total length of 22 cm and inside diameters of 1.17 and 1.45 mm. The effective heating length was 16 cm. The demand curves of the pressure drop versus mass flux were obtained, and the OFI data was compared with the widely used correlations. Stoddard et al. [4] performed the study on the onset of flow instability in heated thin annular flow passages cooled by subcooled water with the inside diameter of 6.4 mm, annular gap widths of 0.724–1.001 mm. As to the authors knowledge, up to now, there are no articles dealing with the onset of flow instability in parallel microchannels. Recently, Qu and Mudawar [5] performed observations by microscope with parallel microchannels and showed that it is difficult to identify specific points such as ONB and OSV. However, they used the term "boiling incipience" instead of these terms, including the fine bubble nucleation and departure phenomena.

1.2. Dynamic flow instability

Dynamic flow instability generally reflects the feed back control process of a combined set of parameters. For large channels, it is commonly recognized that three typical oscillations exist in the boiling or condensation system: pressure drop type oscillation, density wave oscillation and thermal oscillation [6]. Also, there is no conclusion about the dynamic flow instability in microchannels at this stage. Peles et al. [7] deal with forced liquid flow in heated microchannels, dividing the whole flow domain into the liquid part and the vapor part. The model consists of a number of non-dimensional parameters, such as *Pe*, *Ja* and dimensionless heat flux. The experimental findings, combined with the model predictions, show that evaporating flow in microchannels with mean outlet vapor mass quality less than unity is unsteady, and has two distinct domains, one for the liquid and the other for the very short section of vapor. Thus, a vapor mass quality less than unity means alternating outlet phase with mean vapor quality less than one.

Brutin et al. [8] conducted a two phase instability experiment in a single rectangular microchannel with hydraulic diameter of 899 μm. In terms of the operating conditions, two types of behavior were observed: a steady state characterized by low amplitude oscillation of the pressure drop and no characteristic frequency and the other is unsteady two phase flow. The pressure drop exhibits large amplitude oscillations and frequencies ranging from 3.6 to 6.6 Hz.

Very recently, Wu and Cheng [9] studied boiling heat transfer in silicon microchannels with channel hydraulic diameters of 158 and 83 μm. The study shows that once boiling heat transfer is established, single phase liquid flow and two phase flow appear inside the channel alternatively. The measured pressure drop, wall temperatures, inlet and outlet fluid temperatures and mass flux are found to be oscillating with long period/large amplitude. They concluded that such unsteady flow can be self sustained if the pressure drop and mass flux are out of phase.

The present paper consists of two parts. The first one is to acquire the onset of flow instability through the demand curves of the pressure drop versus mass flux at different given inlet liquid temperatures and heating powers. The second part deals with the dynamic instabilities in multi-microchannels.

2. Experimental apparatus and procedure

2.1. Test facility

As shown in Fig. 1, deionized water or methanol was pumped from the liquid reservoir to the test section, through a 15 μm filter. The outlet fluid was condensed by a water cooled condenser and passed to a dual glass rotor flowmeter unit and back to the liquid reservoir. An electronic heater was immersed in the liquid reservoir with a PID temperature control unit, to obtain any desired liquid temperature inside the liquid tank. The 15 μm filter was used to prevent any solid particles from entering the microchannel heat sink. Depending on the flow rate, one of the two water flowmeters was used. The flowmeters were calibrated by weighing the outlet liquid over a given period of time using a high accuracy electronic balance, with both water and methanol as working fluids. The electronic balance has an accuracy of 0.01 g. The inlet liquid temperature of the test section was controlled by setting the PID temperature control unit, and the total flow rate

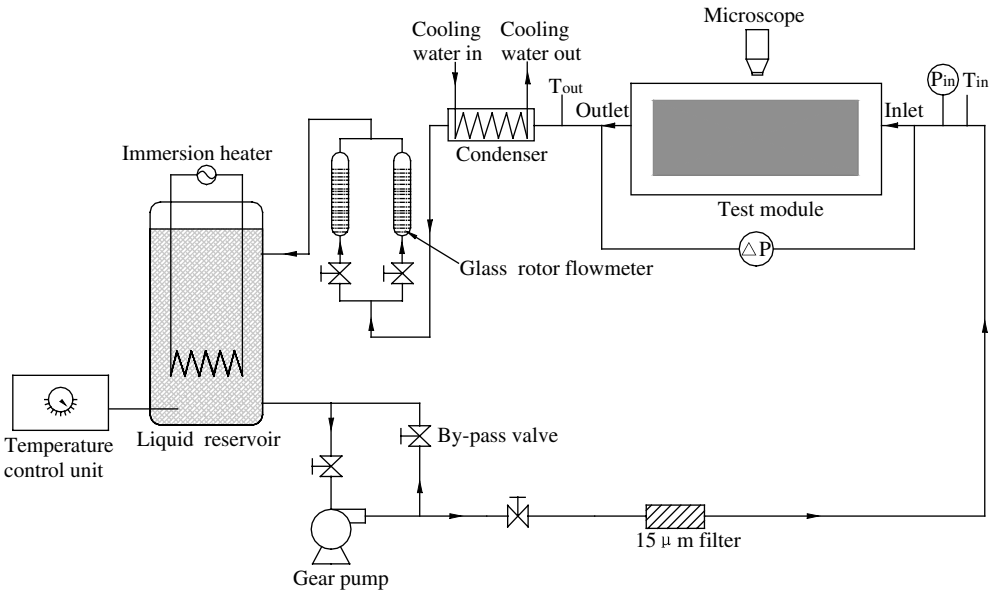

Fig. 1. Experimental test loop.

was obtained by adjusting the valve located in the bypass line and the throttling valve upstream of the microchannel test section.

The inlet and outlet fluid temperatures were measured by high precision jacket thermocouples with a diameter of 1.0 mm, having measurement accuracy within ±0.2 °C after calibration using the constant temperature bath. The response time is estimated to be 50 ms, which is fast enough to trace the dynamic parameters for the present study. The inlet fluid pressure was measured by a Setra pressure transducer (Model 206), which was calibrated against a known standard and the uncertainty in the pressure measurements was less than 0.1%. The pressure drop across the test section was measured by a Senex differential pressure transducer with an accuracy of ±0.1% and a response time of 10 ms. All temperature, pressure and differential pressure signals were collected by a HP high speed data acquisition system and displayed by a PC monitor and stored in PC memory for future analysis.

2.2. Test module

The test module is shown in Fig. 2a for the three dimensional view and Fig. 2b for the detailed technical drawing. It consists of a parallel microchannel heat sink with an O-ring slot, a glass cover plate and a cartridge heater. There are a total of 26 microchannels with 300 μm width and 800 μm depth for each microchannel. The planform (top) surface of the heat sink was 1.53 cm wide and 5.0 cm long. An 8.0 mm diameter hole was drilled in the copper block to accommodate the cartridge heater, with a length of 5.0 cm, exactly the same as the effective length of the microchannels. The cartridge heater was powered by a 0–220 V AC variac, and the heating power was measured by a precision wattmeter, with an accuracy of 0.5%. Six K type thermocouples were

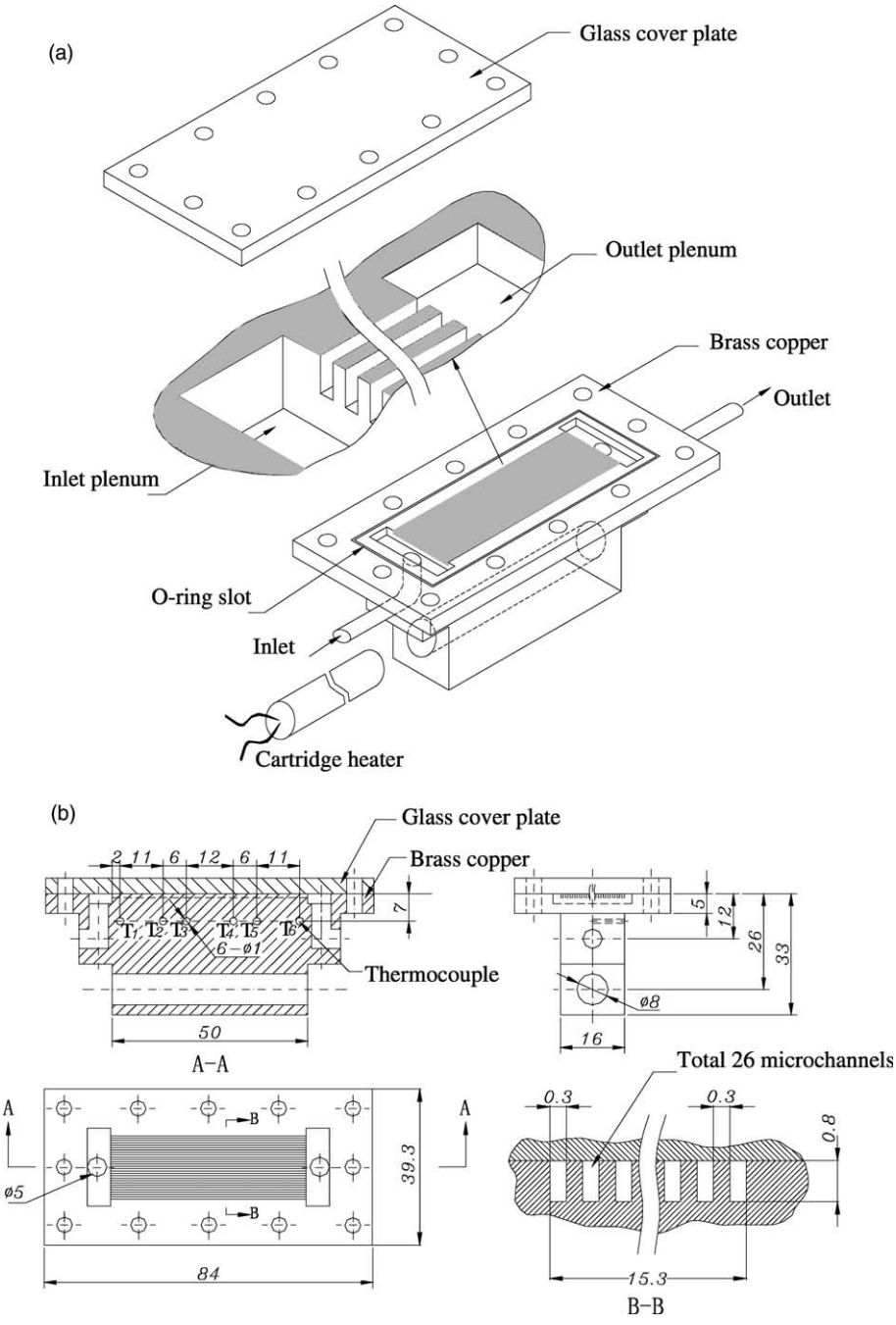

Fig. 2. (a) Three dimensional view of the copper heat sink. (b) Detailed technical drawing of the copper heat sink.

inserted below the heat sink to measure the axial temperature distribution inside the heat sink. The locations are illustrated in Fig. 2b.

A cover plate made from transparent polycarbonate plastic (Lexan) was bolted to the copper heat sink. An O-ring slot was machined in the top surface of the copper heat sink, which served to prevent any leakage from the microchannel slots. A microscope was situated above the cover plate to observe the bubbles in the microchannels, as illustrated in Fig. 1. The copper heat sink was heat insulated using high quality thermal insulation material.

Before performing the two phase flow experiment, a series of single phase liquid flow tests were conducted. Comparison between the electrical power input and the liquid enthalpy increase during the single phase tests proved that the heat loss is less than 5%, and thus the effective heat extracting efficiency is estimated to be 95%. All heat fluxes were, therefore, based on the measured electrical power times the coefficient of 0.95, giving conservative values.

2.3. Experimental procedure

Prior to performing a test, the liquid inside the reservoir was heated to the desired high temperature and maintained at such temperature for a half hour to remove any dissolved gas from the liquid to the ambient. Afterwards, the liquid reservoir was controlled by the PID control unit to yield the desired inlet temperature of the microchannel heat sink, T_{in}. The mass flux through the microchannel can be computed as

$$G = \frac{V}{NA_C} \tag{1}$$

where V is the volume flow rate from the glass rotor flowmeter, N is the number of microchannels, A_C is the cross-section area of each microchannel. Once stable T_{in}, Q (effective heating power) and G are obtained, a steady single phase liquid flow is established. The initial run case was performed for the larger G. Decreasing G will lead to smaller pressure drops until the unsteady two phase flow occurs. The system will stay at each run case for 1 h to ensure stable liquid flow or periodic two phase flow conditions.

The effective heat flux is determined by the effective heating power divided by the top planform area.

$$q_{eff} = \frac{Q}{A_t} \tag{2}$$

where $A_t = 1.53 \times 5.0\ cm^2$. The test parameters are as follows: inlet liquid temperature, T_{in}: 30, 50 and 70 °C; mass flux, G: 20–1200 kg/m^{2}s; effective heating power, Q: 140–450 W; working fluids: water and methanol.

3. Data reduction

The data reduction process involves the heat transfer coefficients along the flow direction. The heat transfer coefficients were only computed for the single phase liquid flow. For the periodic two phase flow, the thermal (wall temperature) oscillations were detected. The dynamic heat transfer coefficients are quite difficult to obtain.

To evaluate the heat transfer coefficient of the single phase liquid flow, a two dimensional unit cell consisting of a single rectangular microchannel and surrounding solid was examined along the flow direction where the thermocouple wires are located. Fig. 3 illustrates the two dimensional unit cell, and the dimensions are given in Table 1. Because it is difficult to obtain the heat transfer coefficients around the perimeter of the microchannel cross-section, a mean heat transfer coefficient, h_{tp}, averaged over the heated perimeter of the microchannel, was acquired using the fin analysis method, which was based on Qu and Mudawar [10].

The fin analysis method applied to the two dimensional unit cell illustrated in Fig. 3 gives the following energy balance equation:

$$q_{eff} W_{cell} = h_{tp}(T_{w,in} - T_f)(W_{ch} + 2\eta H_{ch}) \tag{3}$$

The left hand side of Eq. (3) is the heat input to the unit cell, while the right hand side represents the heat absorbed by the single phase liquid, neglecting the heat loss through the glass cover plate. The fin efficiency is computed as

$$\eta = \frac{\tanh(mH_{ch})}{mH_{ch}} \tag{4}$$

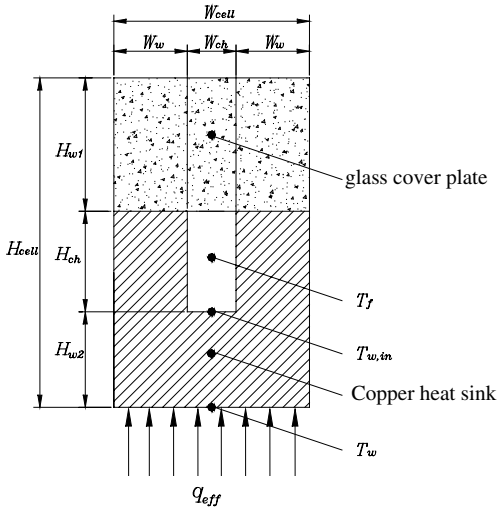

Fig. 3. Two-dimensional microchannel heat sink unit cell.

Table 1
Dimensions of unit cell

W_w (μm)	W_{ch} (μm)	H_{w1} (μm)	H_{ch} (μm)	H_{w2} (μm)
150	300	6200	800	4000

where m is the fin parameter,

$$m = \sqrt{\frac{h_{tp}}{k_s W_w}} \tag{5}$$

where k_s is the thermal conductivity of the solid copper block. $T_{w,in}$ is the temperature of the channel bottom wall, which can be computed using the one dimensional heat conduction equation.

$$T_{w,in} = T_w - \frac{q_{eff} H_{w2}}{k_s} \tag{6}$$

Once $T_{w,in}$ and T_f are decided, h_{tp} can be calculated from Eq. (3) iteratively.

4. Results and discussion

4.1. Onset of flow instability (OFI)

For large channels, the demand curve of the total pressure drop against mass flux at the given inlet liquid temperature and thermal load is given in Fig. 4. Subcooled single phase liquid flow is maintained in the channels until the mass fluxes are decreased to the value at which the measured demand curve deviates from the computed one, accounting for the liquid viscosity variation versus liquid temperature. Such point in the demand curve is identified as the onset of nucleate boiling (ONB). Further continuous decreasing of the mass flux leads to the onset of significant void (OSV), occurring at a slightly higher mass flux than the onset of flow instability (OFI). The

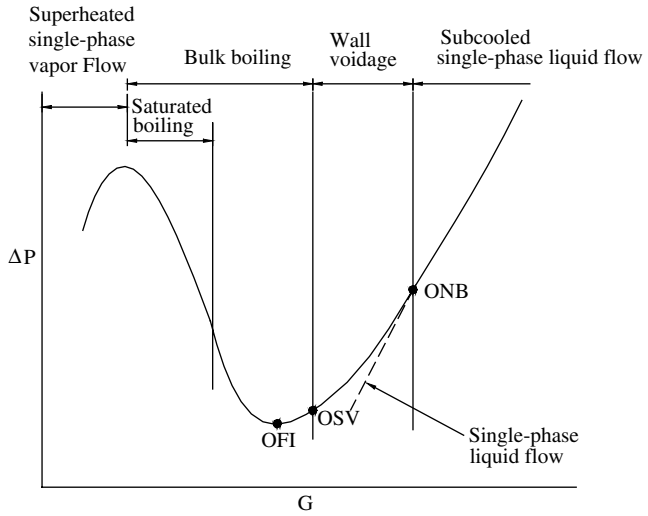

Fig. 4. Demand curve of pressure drop versus mass flux at the given inlet temperature and heating power for large channels.

OFI is at the minimum point of the pressure drop versus mass flux curve. As described in Section 1, no study was reported on the onset of flow instability for multi-microchannels.

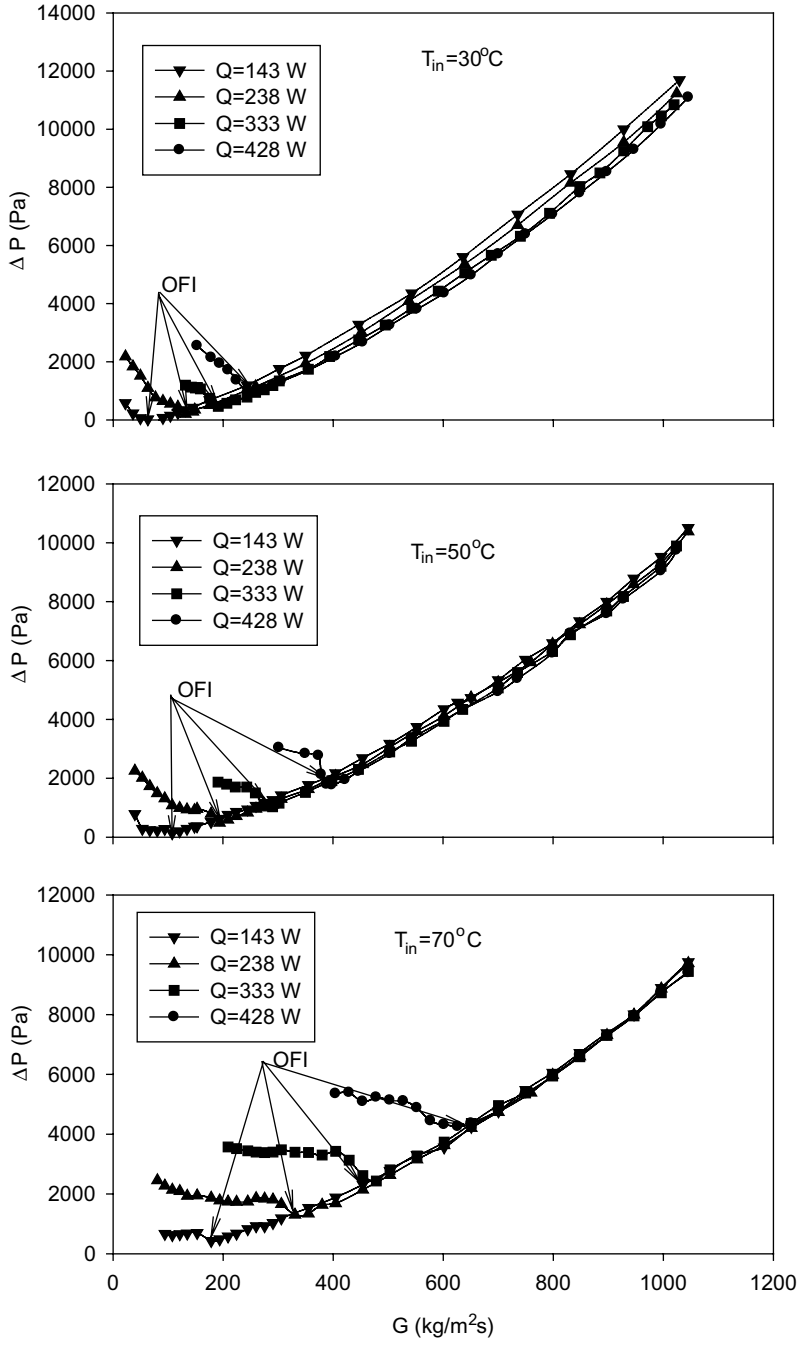

Fig. 5. Demand curve of pressure drop versus mass flux for different inlet liquid temperature and heating power.

Totally, 12 demand curves of the pressure drop versus mass flux were obtained with water as working fluids, as shown in Fig. 5 in which the OFI is marked for each of these curves. Higher mass fluxes than that of the OFI result in single phase liquid flow, while lower mass fluxes than that of the OFI lead to periodic unsteady two phase flow, which will be explained in the next section. The pressure drop and mass flux are obtained using time averaged values for the unsteady two phase flow region.

At low inlet liquid temperatures, such as 30 °C, for a given mass flux, the pressure drop is higher for lower heat input due to the higher liquid viscosity. However, such demand curves for the single phase liquid flow region are approaching the same for the different heating powers at higher inlet liquid temperatures. The OFI occurs at higher mass flux for larger heating power. For lower inlet liquid temperature and smaller heating power, the OFI occurs at a very small pressure drop. The 12 typical OFI run cases are shown in Table 2 for the static parameters, including the inlet pressure, P_{in}; inlet liquid temperature, T_{in}; outlet fluid temperature, T_{out}; mass flux, G; and pressure drop, ΔP.

Simple and purely empirically correlations for the onset of flow instability can be developed by comparing the flow and boundary conditions with those resulting in saturation [3]. The value of heat flux that initiates the saturated liquid condition at the channel exit can be calculated as

$$q''_{sat} = \frac{NGA_C(h_{f,sat} - h_{in})}{A_t} \tag{7}$$

The effective heat flux at the OFI condition can be best correlated with that of a saturated exit condition within 3.39% with 99% confidence as

$$q_{eff,OFI} = 3 + 0.834q''_{sat} \tag{8}$$

where the units of the heat flux are in W/cm^2. The mass flux at the OFI, G_{OFI}, can also be compared with that of a saturated condition, G_{sat}, using the energy balance equation.

$$G_{sat} = \frac{q_{eff}A_t}{NA_C(h_{f,sat} - h_{in})} \tag{9}$$

Table 2
Summary of OFI data

Run case	Q (W)	q_{eff} (W/cm^2)	P_{in} (bar)	T_{in} (°C)	T_{out} (°C)	G (kg/m^2 s)	ΔP (Pa)
1	428	55.8	1.047	30.4	93.2	260	943
2	333	43.5	1.031	29.7	96.5	191	468
3	238	31.1	1.053	29.9	95.6	136	205
4	143	18.7	1.021	30.6	96.6	82	36
5	428	55.8	1.060	50.2	93.2	382	1729
6	333	43.5	1.047	50.1	93.4	291	1030
7	238	31.1	1.031	50.1	96.5	194	486
8	143	18.7	1.028	50.2	95.9	115	138
9	428	55.8	1.115	70.5	96.0	629	4250
10	333	43.5	1.076	70.0	96.4	479	2435
11	238	31.1	1.049	70.2	96.7	333	1305
12	143	18.7	1.032	69.2	98.4	179	434

The results show that the mass flux at the onset of flow instability can be predicted from the following equation within 2.83% with 98% confidence, as

$$G_{\mathrm{OFI}} = 1.17 G_{\mathrm{sat}} \tag{10}$$

Fig. 6 shows a typical run case for the OFI condition. It is seen from the figure that all six wall temperatures where the six thermocouple wires are located are larger than the saturated temperature of 100 °C corresponding to the exit pressure. However, the computed bottom wall temperatures at the entrance region for $T_{\mathrm{w,in1}}$ and $T_{\mathrm{w,in2}}$ are less than 100 °C. Other temperatures

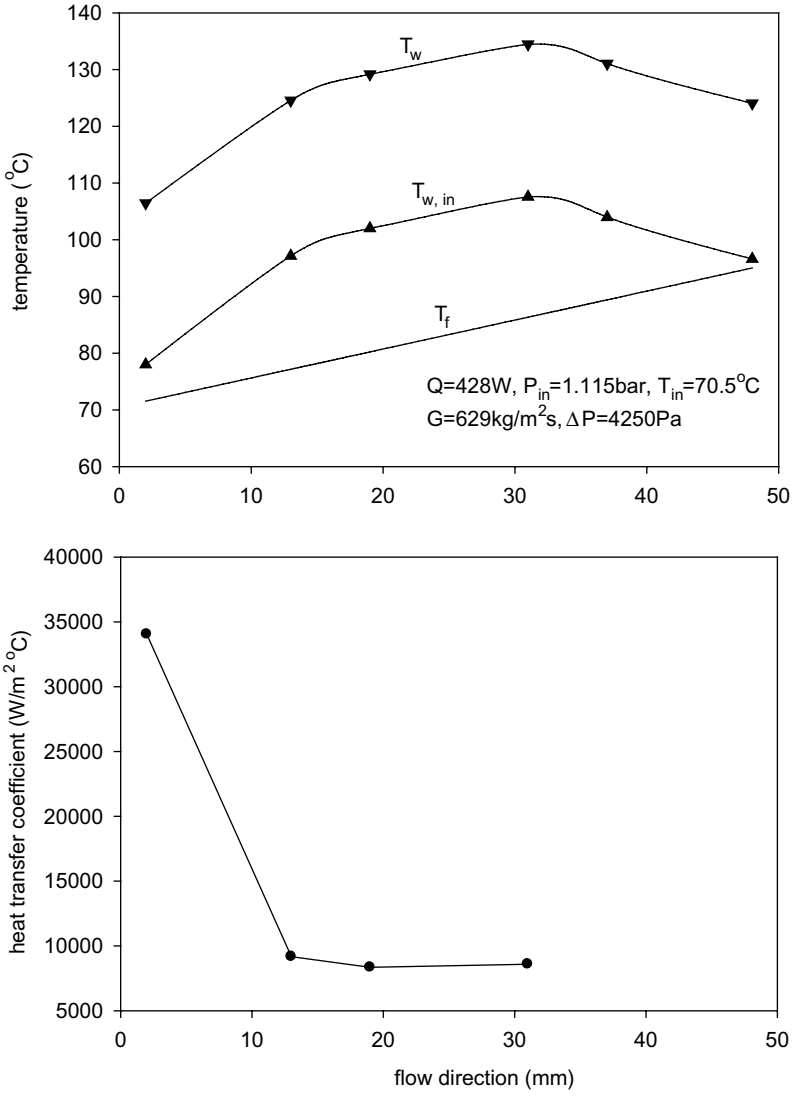

Fig. 6. Fluid temperature, wall temperatures and heat transfer coefficients along the flow direction at a typical OFI run case.

downstream of $T_{w,in2}$ are larger than 100 °C. The entrance region from point 1 to 2 has smaller temperature differences between the bottom wall surface and the local fluid. Thus, higher heat transfer coefficients are obtained, possibly due to the developing thermal boundary layer. The variations of bottom wall temperatures along the flow direction from point 2 to 4 are parallel to the increase of fluid temperature, leading to the near constant heat transfer coefficients around 8400–9200 W/m^2 °C, indicating the developed thermal boundary layer in this region. The heat transfer coefficients for points 5 and 6 close to the microchannel exit have large errors, and thus, they are not shown in the figure.

4.2. Observations at OFI

Physically, the onset of nucleate boiling (ONB) is the condition at which fine bubbles begin to be activated in the cavity adjacent to the solid wall. Such fine bubbles may be tightly attached to the wall surface. The flow may be continued downstream of the ONB, until the bubbles begin to depart from the wall surface and form significant voids in the main flow (OSV). The above description is suitable for large channels. When the channel hydraulic diameter is reduced, satisfying the criterion of $D_e = \sqrt{\sigma/g(\rho_f - \rho_g)}$, it is very difficult to identify the differences between the ONB and the OSV. Experimental work by Qu and Mudawar [5] indicates that the bubble behavior at the boiling incipience in microchannels is quite different from that in large channels. They observed that fine bubbles appear close to the exit of several microchannels. Some of them were on the bottom wall, but a few were also observed on the side wall at the boiling incipience point. After nucleation, the bubbles first grew to depart from the wall surface. The detached bubble sizes are comparable with the channel hydraulic diameter. The detached bubbles are flowing to the exit plenum where they collapse. Based on these observations, they suggest that boiling incipience be used instead of the ONB and the OSV.

The present observations generally conform with those performed by Qu and Mudawar [5]. However, when the fine bubbles close to the exit of the microchannels arrived at the exit plenum, they were quickly coalesced instead of collapsed. Therefore, we always observed a single larger circular bubble in the center of the exit plenum with a diameter of 2–3 mm. Such bubble phenomena do correspond to the flow condition at the OFI. Therefore, roughly, the boiling incipience defined by Qu and Mudawar [5] can correspond to the OFI condition, which can be determined through the demand curve of the pressure drop against the mass flux. For the present experiment, using water as the working fluid, the OFI occurs at an outlet fluid temperature from 93 to 96 °C, which is less than the saturated temperature of 100 °C, corresponding to the exit pressure, by 4–7 °C.

4.3. Oscillation flow and heat transfer in microchannels

Once the mass flux is less than that of the OFI, three types of oscillations appear: large amplitude/long period oscillation (LALPO), small amplitude/short period oscillation (SASPO) and thermal oscillation (TO). The thermal oscillations are always identified as accompanying the other two oscillation flows.

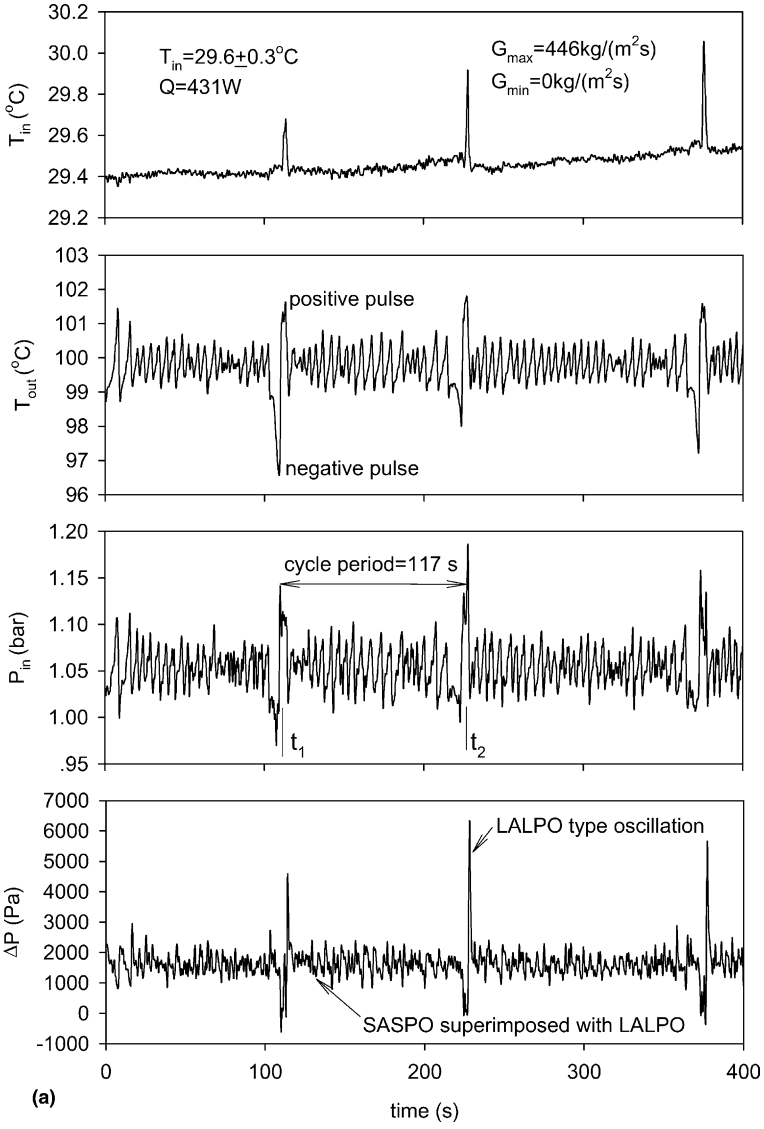

Fig. 7. (a) Recordings of T_{in}, T_{out}, P_{in} and ΔP versus time for the LALPO type oscillation superimposed with SASPO type oscillation. (b) Recordings of wall temperatures versus time for the LALPO type oscillation superimposed with SASPO type oscillation.

4.3.1. LALPO type oscillations superimposed with SASPO

LALPO type oscillations occur at the lower inlet liquid temperature of 30 °C, superimposed upon SASPO type oscillations. Fig. 7a and b show the recordings of T_{in}, T_{out}, P_{in}, ΔP and T_{w1}–T_{w6} against time for the heating power of 431 W (corresponding heat flux of 56.3 W/cm^2). Because the volume flow rate is measured by one of the two glass rotor flowmeters, it cannot be recorded by the computer automatically. However, observations by the naked eye show that the flow rate is

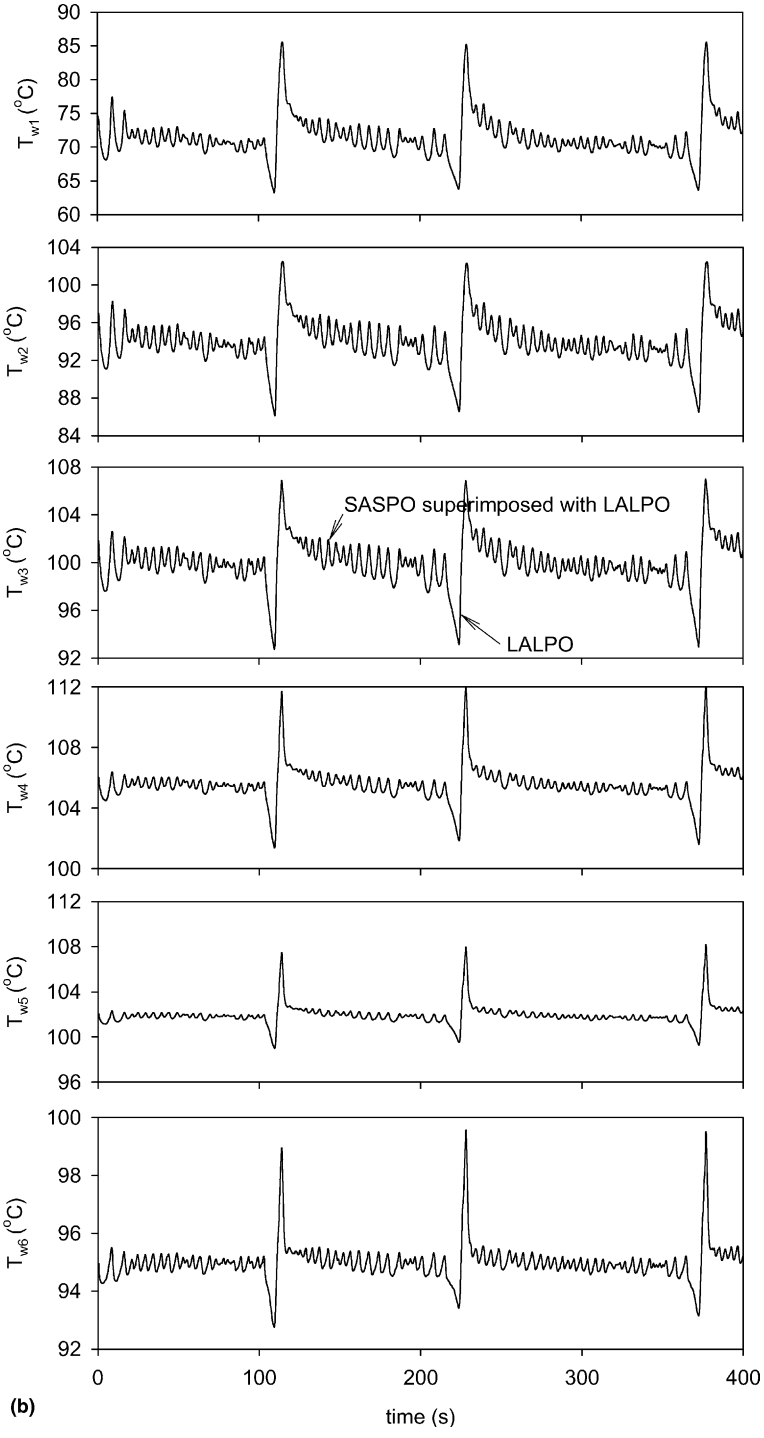

Fig. 7 (*continued*)

oscillating in the range from the maximum value of 446 kg/m^2 s to the minimum value around zero periodically. A typical full cycle for the LALPO type oscillation is identified from t_1 to t_2, covering the time period of 117 s (nearly 2 min). All the parameters have large oscillation amplitudes, for example, T_{out} varies from 96 to 101 °C, P_{in} varies from 0.96 bar (below environment pressure) to 1.2 bar, ΔP oscillates from −800 Pa (negative pressure drop indicating back flow upstream of the microchannels) to 5000–6000 Pa. All six wall temperatures are oscillating simultaneously with oscillation amplitudes up to 10 °C (defined as the peak values against the mean averaged ones).

The observations through the microscope around the time at which the microchannels switch from one large cycle to a another new cycle, for instance around t_1 or t_2, indicate that suddenly fresh liquid invades and occupies the whole microchannels, leading to sharp decreases of the outlet temperature (T_{out}), inlet pressure (P_{in}) and pressure drop (ΔP). The initial bubbles existing in the microchannels are observed to be quickly condensed by the flushing liquid and collapsed. However, the quick inburst of the entrance liquid process takes about a couple of seconds, which is then followed by sharp bulk boiling of the microchannels. The vapor produced in the microchannels expands both upstream and downstream of the microchannels, resulting in sharp positive pulses of the outlet and inlet temperatures. Afterwards, the microchannels evolve to the SASPO type oscillation imposed on the above described LALPO type oscillations, which will be discussed later. During the short bulk vapor expansion period, the sharp positive pulse of the inlet liquid temperature identifies the strong back flow of the vapor that penetrates to the inlet thermocouple tip. The wall temperatures of T_{w1}–T_{w6} follow the dynamic variations of other parameters, such as T_{out}, P_{in} and ΔP, that is, sharp negative pulses followed by positive pulses. The negative pulses of the wall temperatures are coming from the higher heat transfer coefficients and the lower liquid temperature in the microchannel during the entrance fresh liquid flushing period. The following positive pulses of the wall temperatures result from the lower heat transfer coefficients and the higher saturated or slightly superheated vapor in the microchannels.

The power spectral density (PSD) is usually applied to extract the periodic feature of a signal. Wang et al. [11] computed the PSD of the differential pressure fluctuations to distinguish the two phase flow through the T-junctions between periodic and chaotic motion. If the power spectrum is continuous and asymptotic, the motion can be considered as chaotic [12]. However, if the power spectrum only has a sharp peak distribution at a dominant characteristic frequency, the motion can be considered as periodic. In the present paper, the PSD is applied to analyze the dynamic signals shown in Fig. 7a and b. The calculation performed using MATLAB shows that there are two dominant frequencies, one is 7.87×10^{-3} Hz (117 s), corresponding to the LALPO oscillation flow and the other is 0.197 Hz (5.08 s), corresponding to the superimposed SASPO oscillation flow.

4.3.2. SASPO type oscillation

The microchannels behave with SASPO type oscillations at the higher inlet liquid temperatures. Typical parameter recordings of T_{in}, T_{out}, P_{in} and T_{w1}–T_{w6} are shown in Fig. 8a and b for the inlet liquid temperature of 50 °C and heating power of 331 W (the corresponding heat flux is 43.3 W/cm^2). The mass flux varies from 0 to 543 kg/m^2 s. The oscillation cycle period is estimated to be 10.3 s, which is one order of magnitude less than the long period of 100 s for the LALPO type oscillations. These parameters are oscillating with small amplitudes, except the stable recordings of T_{in}. A full cycle can be defined from $t = t_A$ across $t = t_B$ to $t = t_C$. The outlet temperature, T_{out},

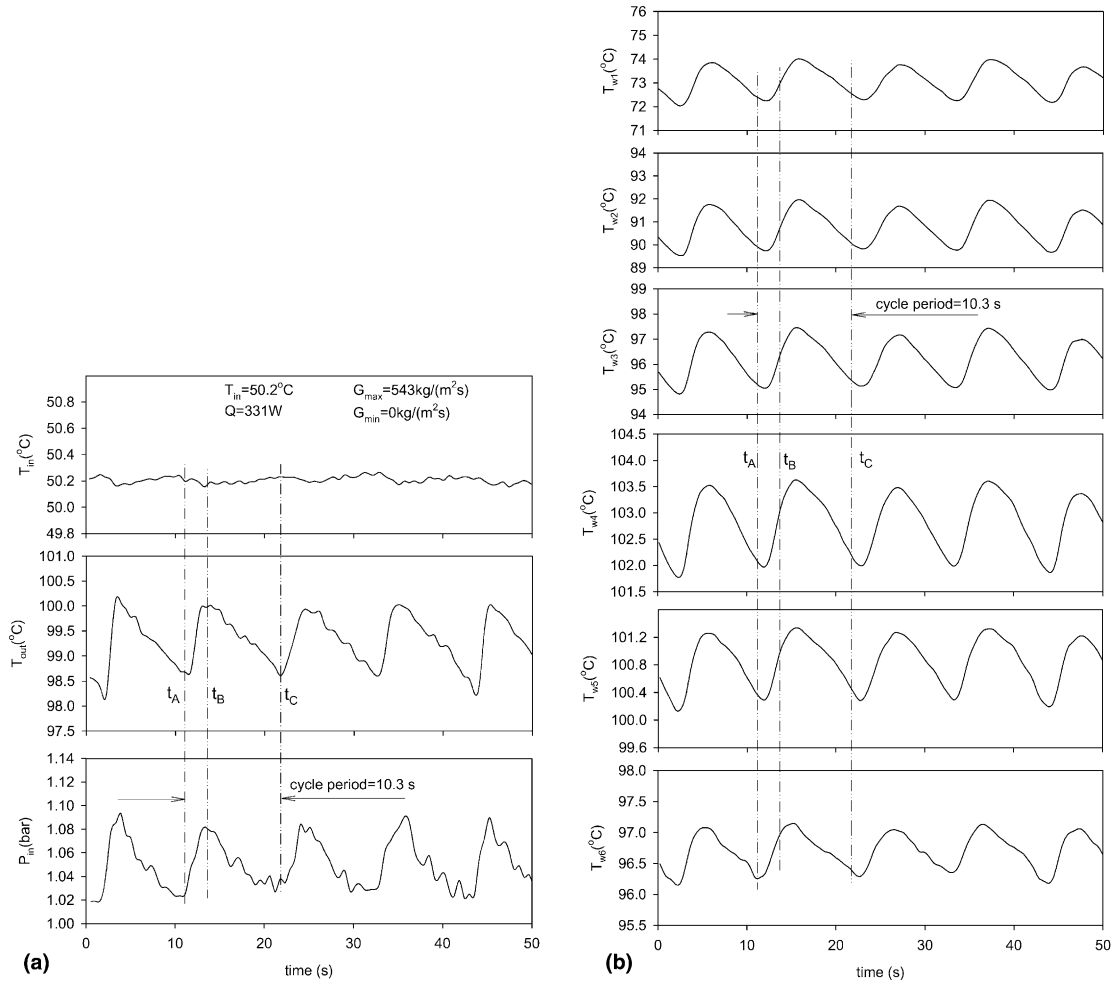

Fig. 8. (a) Recordings of T_{in}, T_{out} and P_{in} versus time for the SASPO type oscillation. (b) Wall temperature recordings versus time for the SASPO type oscillation.

has a sharp increase from $t = t_A$, obtains the peak value at $t = t_B$ and then follows a decrease until $t = t_C$, with the oscillation amplitude (defined as the peak value against the average one) of 1 °C. The inlet pressures oscillate, corresponding to the outlet temperature, in phase, varying from 1.02 to 1.08 bar (oscillation amplitude is 0.03 bar).

The six wall temperatures also vary periodically. However, they have slight phase angles. Surprisingly, we did find that T_{w6}, which is close to the exit of the microchannels, increased from the minimum value at $t = t_A$ to the peak value at a time a little beyond $t = t_B$ and then decreased from the peak value to the minimum around $t = t_C$, matching the oscillation trends with the outlet temperature and the inlet pressure. The other wall temperatures, except T_{w6}, roughly match the dynamic trends with the outlet temperature T_{out} and the inlet pressure P_{in}. However, they have time delays relative to those of T_{out} and P_{in}, indicating the thermal inertia of the solid copper block. From Fig. 8b, one can also detect the axial temperature distributions. Generally, among all the six wall

temperatures, T_{w1} is the lowest but the temperatures increase along the flow direction until the maximum temperature at T_{w4} is reached. Further downstream of T_{w4}, the wall temperatures are decreased due to axial heat conduction inside the copper block. The maximum temperature of T_{w4} has the time averaged value of 102.7 °C, which is around 3° higher than that of the saturated temperature at the environment pressure. In other words, even though the microchannel is in the dynamic state and the wall temperatures vary periodically, the solid wall is well cooled for the SASPO flow.

4.3.3. Observations of the SASPO type oscillations

Because the oscillation period is up to 10 s, observations through the microscope are possible to be performed. Corresponding to a full cycle from $t = t_A$ across $t = t_B$ to $t = t_C$ shown in Fig. 8a and b, the observations are shown in Fig. 9 and described as follows:

(1) At the time around t_A, fine bubbles are observed very close to the exit of the microchannels, whose diameters are the same order as the hydraulic diameter of the microchannel. In the outlet plenum of the microchannel, a unit circular bubble is observed with a bubble diameter of 2–3 mm (shown in Fig. 9). Such bubble phenomena are similar to those of the OFI condition.
(2) In the stage of $t_A < t < t_B$, as shown in Fig. 9, the vapor–liquid interface (boiling front) is moving upstream in the microchannels. Roughly, the vapor–liquid interface is dividing the whole microchannel into two regions, the liquid region and the two phase region. Because of the surface tension effect in the microchannels, the flow pattern in the two phase region is a vapor slug, or annular flow with the vapor core in the channel center but a thin liquid film between the perimeter and the center vapor core.
(3) At $t = t_B$, the vapor–liquid interface of some microchannels (not all) arrived at the channel inlet. Because the liquid in the inlet plenum is "cold", a strong condensation effect takes place at the vapor–liquid interface, causing the shrinking of the vapor slug.
(4) Following $t > t_B$, the vapor–liquid interface is moving downstream in the microchannel (normal flow direction). Because of the shrinkage of the vapor slug, the inlet pressure is decreased. The observed mass flow rate is increased. Because of the increased mass flux and the fresh liquid recovered in the microchannel, the heat transfer coefficients are increased, and thus, the wall temperatures are decreased until $t = t_C$ is reached where a new cycle begins.

4.3.4. SASPO type oscillation for methanol

In order to check the two phase flow and heat transfer behavior in microchannels with other working fluids, an unsteady flow experiment was performed using methanol as working fluid. Because the single phase liquid flow and heat transfer is beyond the scope of the present paper, we only present a typical run case for the periodic flow for the inlet liquid temperature of 28 °C and heating power of 307 W. The computed mass flux observed from the glass rotor flowmeter varies from 936 kg/m^2 s to zero. The physical properties of water and methanol at a 1 atm saturated condition are shown in Table 3. It is seen from Fig. 10a and b that (1) all the parameters, except T_{in}, are self sustained oscillating at the same cycle period. (2) The inlet temperature is stable indicating the back flow cannot penetrate to the inlet thermocouple tip. (3) The outlet temperature

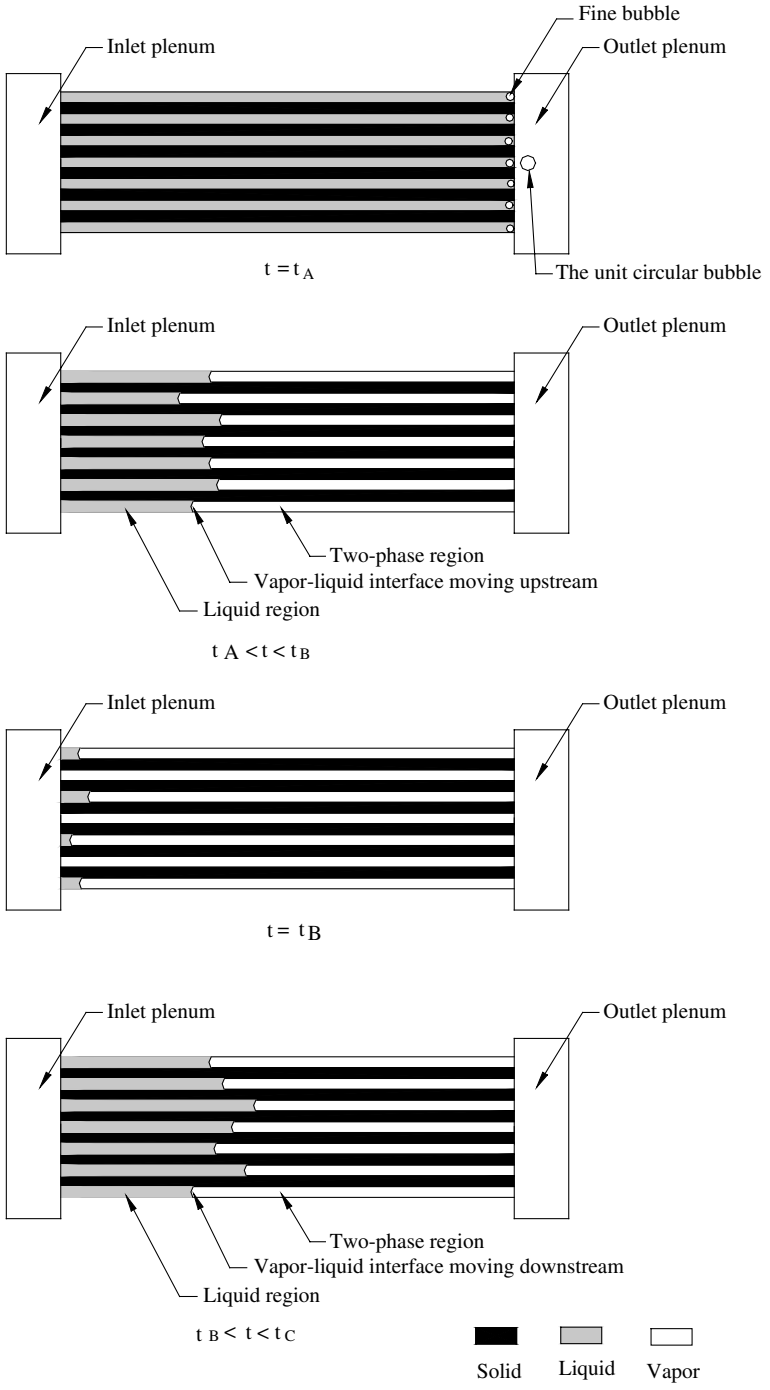

Fig. 9. Dynamic vapor–liquid interface for the SASPO type oscillation.

Table 3
The physical properties of water and methanol at 1 atm saturated condition

Working fluids	T_{sat} (°C)	ρ_f (kg/m^3)	ρ_g (kg/m^3)	$C_{P,f}$ (J/(kg °C))	H_{fg} (kJ/kg)	σ (N/m)
Methanol	64.8	747	1.418	2621	1110	18.5×10^{-3}
Water	100	958	0.6	4217	2257	58.9×10^{-3}

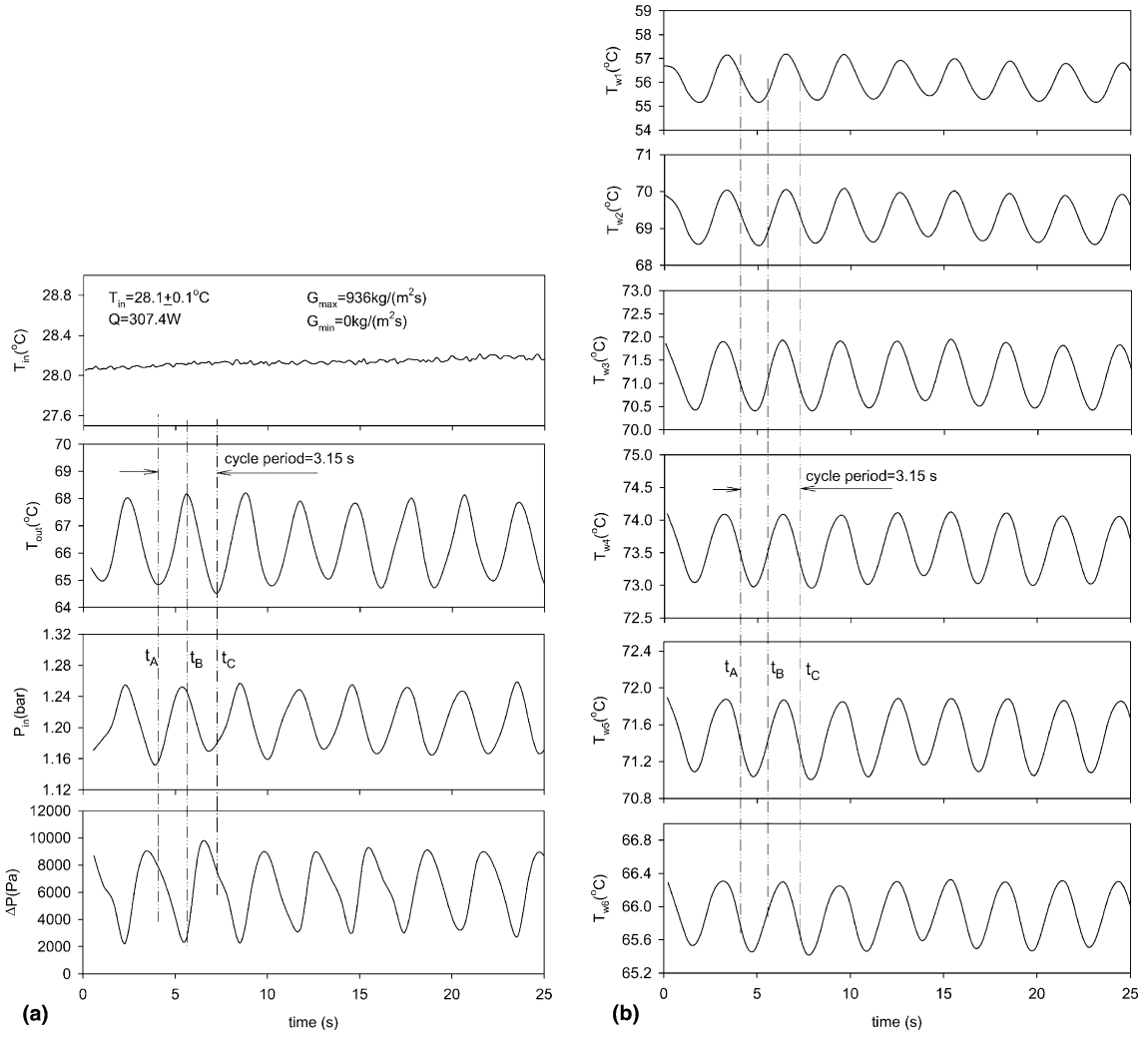

Fig. 10. (a) Recordings of T_{in}, T_{out}, P_{in} and ΔP versus time for the SASPO type oscillation (working fluid: methanol). (b) Wall temperature recordings versus time for the SASPO type oscillation (working fluid: methanol).

and the inlet pressure are always in phase, and the wall temperatures generally have the same phase as the others but with some time delay due to the thermal inertia of the copper block. (4) The pressure drop is always out of phase with the other parameters, such as outlet temperature

and inlet pressure. (5) Even though the microchannels have dynamic characteristics, the solid wall is well cooled with the maximum temperature T_{w4} higher than the saturated temperature of methanol by several degrees. (6) Because of the small specific heat and latent heat of evaporation, the time period is estimated to be 3.15 s, which is shorter than that for water with the same other working conditions.

5. Conclusions

From the present experimental work, the conclusions can be summarized as follows:

1. Covering the present parameter ranges, the onset of flow instability occurs at the outlet fluid temperature of 93–96 °C, which is several degrees lower than the saturated temperature corresponding to the exit pressure of the microchannels.
2. The OFI conditions were compared with those of saturation using Eqs. (8) and (10).
3. Observations through the microscope show that once the OFI appears, fine bubbles are found close to the exit of the microchannels, they are moving to form a unit circular bubble in the outlet plenum. Thus, the boiling incipience defined by Qu and Mudawar [5] can correspond to the OFI flow condition.
4. The LALPO type oscillations appear at the lower inlet liquid temperature. It consists of a negative pulse followed by a positive pulse. The negative pulse indicates the "cold" liquid occupies the microchannel, leading to higher heat transfer coefficients. The positive pulse indicates the vapor expands both upstream and downstream of the microchannels, leading to lower heat transfer coefficients. The LALPO type oscillations are always superimposed upon the SASPO type oscillations. Thermal oscillations accompany the oscillation flows.
5. The SASPO type oscillations have small amplitude and short period. The outlet temperature and inlet pressure are always in phase, but they are out of phase with the pressure drop across the microchannels. The wall temperatures generally match the oscillation trends of the inlet pressure and the outlet temperature, but a time delay occurs due to the thermal inertia of the copper block.
6. For one full cycle of the SASPO type oscillation, the observations show that the increasing stage of the outlet temperature and the inlet pressure corresponds to the vapor–liquid interface moving upstream in the microchannels, while the decreasing stage represents the entrance of fresh liquid, pushing the vapor–liquid interface downstream in the microchannels.

Acknowledgements

The authors are thankful for the financial support by the Natural Science Foundation of Guangdong Province, China, with contract number of 32700.

References

[1] Bowers MB, Mudawar I. High flux boiling in low flow rate, low pressure drop mini-channel and micro-channel heat sinks. Int J Heat Mass Transfer 1994;37(2):321–32.

[2] Kandlikar SG. Fundamental issues related to flow boiling in minichannels and microchannels. Exp Thermal Fluid Sci 2002;26:389–407.
[3] Kennedy JE, Roach Jr GM, Dowling MF, Abdel-Khalik SI, Ghiaasiann SM, Jeter SM, et al. The onset of flow instability in uniformly heated horizontal microchannels. ASME, J Heat Transfer 2000;122:118–25.
[4] Stoddard RM, Blasick AM, Ghiaasiaan SM, Abdel-Khalik SI, Jeter SM, Dowling MF. Onset of flow instability and critical heat flux in thin horizontal annuli. Exp Thermal Fluid Sci 2002;26:1–14.
[5] Qu W, Mudawar I. Prediction and measurements of incipient boiling heat flux in microchannel heat sinks. Int J Heat Mass Transfer 2002;45:3933–45.
[6] Ding Y, Kakac S, Chen XJ. Dynamic instability of boiling two phase flow in a single horizontal channel. Exp Thermal Fluid Sci 1995;11:327–42.
[7] Peles YP, Yarin LP, Hetsroni GJ. Steady and unsteady flow in a heated capillary. Int J Multiphase Flow 2001;27:577–98.
[8] Brutin D, Topin F, Tadrist L. Experimental study of unsteady convective boiling in heated minichannels. Int J Heat Mass Transfer 2003;46(16):2957–65.
[9] Wu HY, Cheng P. Visualization and measurements of periodic boiling in silicon microchannels. Int J Heat Mass Transfer 2003;46(14):2603–14.
[10] Qu WL, Mudawar I. Flow boiling heat transfer in two phase micro-channel heat sinks—I. Experimental investigation and assessment of correlations methods. Int J Heat Mass Transfer 2003;46(15):2755–71.
[11] Wang SF, Mosdorf R, Shoji M. Nonlinear analysis on fluctuation of two phase flow through a T-junction. Int J Heat Mass Transfer 2003;46:1519–28.
[12] Cai Y, Wambsganss MW, Jendrzejczyk JA. Application of chaos theory in identification of two phase flow patterns and transitions in a small, horizontal, rectangular channel. ASME, J Fluid Eng 1996;118:383–90.